Article

Not peer-reviewed version

Effective Unidirectional Wetting of Liquids on Multi-gradient, Bio-inspired Surfaces Fabricated by 3D Printing and Surface Modification

Che-Ni Hsu , Ngoc Phuong Uyen Mai , Po-Yu Chen *

Posted Date: 14 May 2024

doi: 10.20944/preprints202405.0926.v1

Keywords: gradient wettability; anisotropic wetting; surface modification; water management

Article

Effective Unidirectional Wetting of Liquids on Multi-Gradient, Bio-Inspired Surfaces Fabricated by 3D Printing and Surface Modification

CheNi Hsu, Ngoc Phuong Uyen Mai and PoYu Chen *

Department of Materials Science and Engineering, National Tsing Hua University, Taiwan;
e-mail@e-mail.com (C.H.); mainpuyen@gmail.com (N.P.U.M.)
* Correspondence: poyuchen@mx.nthu.edu.tw

Abstract: The movement of liquid droplets on the energy gradient surface has attracted extensive attention. Inspired by biological features in nature, such as the periodic spindle-shaped nodes in spider silks and conical-like barbs of cacti, the structure-property-function relationship of multifunctional gradient surfaces. In this study, a series of specific patterns are fabricated by 3D printing technology, followed by modification via the atmospheric pressure plasma treatment and liquid phase chemical deposition, resulting in enhancing the ability of water droplets of 5μL to travel 18.47mm on a horizontal plane and 22.75mm against gravity up to 20° tilting angle. Additionally, analysis techniques have been employed including contact angle analyzer, ESCA and laser confocal microscope to evaluate the sample performance. This work could further be applied to many applications related to microfluidic devices, drug delivery and water/fog collection.

Keywords: gradient wettability; anisotropic wetting; surface modifications

1. Introduction

Controlled self-propelling liquid transport is of considerable interest for specific applications, such as self-cleaning, microfluidic devices, water/fog collection and condensing equipment [1–5]. This field has been well-studied by previous researchers in general [6–11], while Laplace pressure gradient force and wettability gradient from biological properties particularly have drawn much attention as the main driving forces for unidirectional wetting [6,12–20]. For instance, the spine of cacti accumulates fog in humid environment using their barbs, due to the hierarchical cone-like shape, the droplet is driven to move from the tip to the base [12,16]. Periodic spindle knots and joints of spider silks show a series of semitransparent puffs composed of cylindrical silk thread. The fog can be condensed on the silk and driven from the joint to the knot [17,18]. Moreover, the unidirectional wetting behavior of desert beetles has been uncovered with the combination of hydrophilic bumps and hydrophobic channels on the exoskeleton, the droplet accumulates on the bumps and rolls down the beetle back when it overcomes the capillary force [18,19].

Previous studies have been exploiting the natural traits to regulate the liquid spreading combining different geometrical anisotropy and wettable gradients [8,12,15,20–28]. Zhang et al. used an electrospinning technique with a high-speed collection drum to synthesize an aligned PET/CHI fibrous surface, and the resulting parallel structure improves the wetting behaviors [26]. Then, the lifting-dissolution method was applied to the fibrous surface to achieve gradient wettability. The traveling distance of the water droplet on the gradient fibrous surface was 12.3mm with 5μL in volume. Zhu and co-workers took advantage of the beetles' structure, which synthesized a superhydrophilic background by alkaline oxidation to the smooth copper mesh [27]. In a sequence of dipping into the mixer of n-hexane and n-octadecyl thiol/ethanol to achieve the superhydrophobic circular patterns. The efficiency in water capturing was outperformed with 1107.5 $mgh^{-1}cm^{-2}$. Deng et al. used the anodic oxidation method to formulate the wettable gradient surface, which was then

 doi:10.20944/preprints202405.0926.v1

coated with paraffin wax to create a hydrophobic background [28]. A wedge pattern was removed to generate a Laplace pressure gradient on the wettable gradient surface, leading to the water droplets self-transport unidirectionally 2.4mm under the given volume of 5μL.

Our research is motivated by the unique characteristics of cactus and spider silk as mentioned above, we further investigate the anisotropic wetting with an array of triangular prism grooves by 3D printing technology integrating with surface modification, including plasma treatment and polymer grafting, as shown in Figure 1. The wedge-shaped pattern with the Laplace pressure gradient (LG) would drive the droplet from the tip (high LG) to the base of the triangle (less LG) on a wettable gradient surface. Moreover, the multi-gradient surface is sufficient to manipulate the droplet to spread against gravity at varying tilting angles. Besides that, the surface profiles of the patterns were analyzed by laser confocal microscopy, contact angle analyzer and electron spectroscopy for chemical analysis (ESCA). We expect that such a simple and economical design could be a potential work for further research and practical applications for unidirectional wetting.

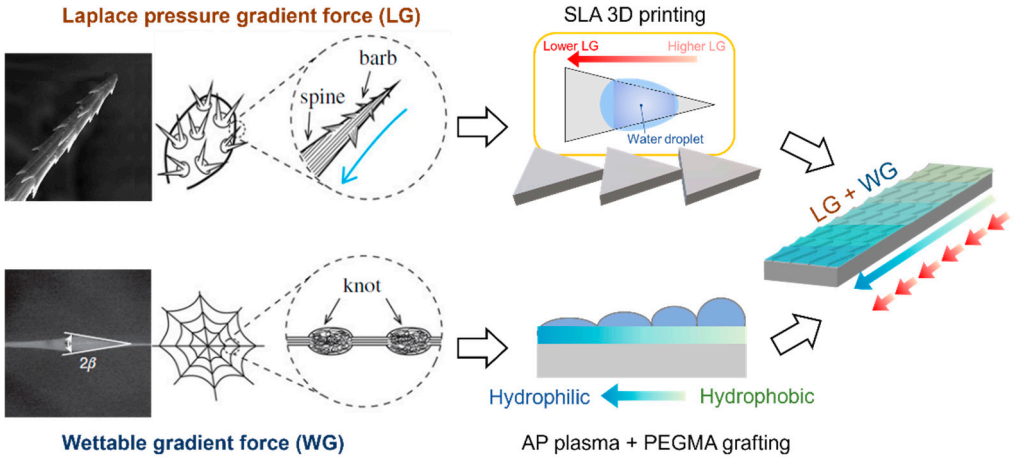

Figure 1. The schematic illustrates the multi-gradient triangular prism pattern. Reproduced with permission. Copyright 2010, Macmillan Publisher Limited, Springer Nature [6]. Reproduced with permission. Copyright 2012, Jie Ju, Springer Nature [12]. Reproduced with permission. Copyright 2016, Philip S. Brown and Bharat Bhushan, Royal Society [19].

2. Materials and Methods

2.1. Preparation of 3D-Printed Triangular Prism Pattern

The design parameters of the structural samples are shown in Figure 2, including 5mm and 1.76mm in length and width of a groove, respectively. The spacing between two extruded wedge-shaped was designated S, the groove's thickness was designated T, and the tip was fixed to an angle of 20°. All samples were printed by a Formlabs2 SLA 3D printer (Formlabs, USA) with liquid ray resin as the printed slurry. The printed samples were then rinsed with isopropanol in an ultrasonic machine for 15 minutes, they ultimately were put into the ultraviolet oven to cure and remove the residual moisture of samples.

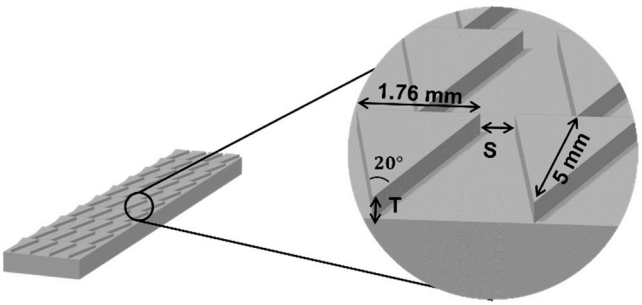

Figure 2. Design parameters of the ABS-like samples with triangular prism patterns.

 doi:10.20944/preprints202405.0926.v1

2.2. Preparation of PEGMA-Grafted 3D Printed ABS-like Samples

For the first step with atmospheric pressure plasma treatment, the printed flat substrates were treated with a certain working distance (non-inclination) and an inclined angle of 20° for the investigation in static contact angle. On the other hand, the structural samples were modified by plasma at a 20° angle. Plasma treatment was introduced to activate and cover the surface with plenty of unstable free radicals and hence perform hydrophilicity and wettable gradient for preparation of the next step.

These plasma-treated sample surfaces were once immersed in PEGMA solution (Mn~440, Alfa Aesar, MA, USA) at 60° for 24 hours to generate a stable wettability state. Finally, the grafted samples were rinsed thoroughly with deionized water in an ultrasonic machine for 10 minutes to eliminate the unreacted PEGMA molecules adhered to the samples, then dried in the oven at 60° for an hour and prepared for the following measurements.

2.3. Water Flow behavior Observation

The experiment was set up with a contact angle analyzer and a digital camera to record the dynamic wetting behavior on the bioinspired-patterned ABS-like surfaces. Colored deionized water droplets of 5-15μL in volume were dropped on the samples at room temperature (24-26°C) and 50-70% relative humidity. The traveling distance and velocity of the water droplets were further analyzed by the ImageJ software (National Institutes of Health, USA). Moreover, the CCD from the contact angle apparatus was used to observe the static contact angle and measure the time-dependent durability of hydrophilicity on the modified flat substrates. At least three individual measurements were performed on each modified sample.

3. Results and Discussion

3.1. Gradient Wettability on Flat ABS-like Substrates

3.1.1. Static Angle Measurement and Dynamic Wetting Behavior

The water contact angle is evaluated on a non-pattern ABS-like substrate with different surface treatments, as shown in Figure 3. The intrinsic contact angle of the 3D-printed ABS-like substrate is 100.1°±1.4°. After being treated by atmospheric pressure (AP) plasma at a working distance of 3.4mm, the contact angle decreases considerably to 12.2°±5.8°. The efficiency in hydrophilic of the plasma-treated surface is examined within 30 days in Figure 4. Unfortunately, the plasma-treated sample reaches 95.1°±2.2° of contact angle, which seems to recover to its initial state in the first 7 days, because the effect of plasma is to generate active species, which spark diffusing from the bulk surface toward the inner side and cover the thermodynamically unstable surface [29]. To address that drawback, the plasma-treated one is further immersed in PEGMA solution, resulting in a contact angle that continues reducing to 11.1°±0.8°. Moreover, the hydrophilicity of PEGMA-grafted ABS-like substrate could maintain at least 30 days at 12.3°±2.7° on average, successfully sustaining a hydrophilic state. The long-term durability of hydrophilicity is reckoned with the stable bonding between functional groups of PEGMA and plasma-treated ABS-like surface, which is proved by ESCA in the next section.

 doi:10.20944/preprints202405.0926.v1

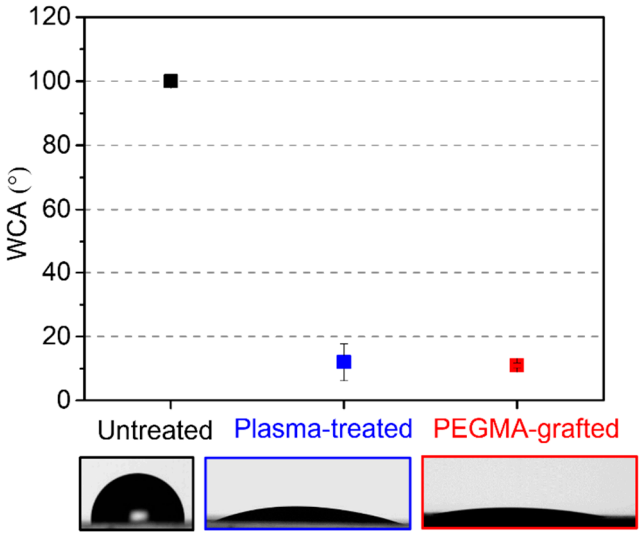

Figure 3. The plot of the water contact angle versus untreated, plasma-treated, and PEGMA-grafted samples corresponds with the CCD images.

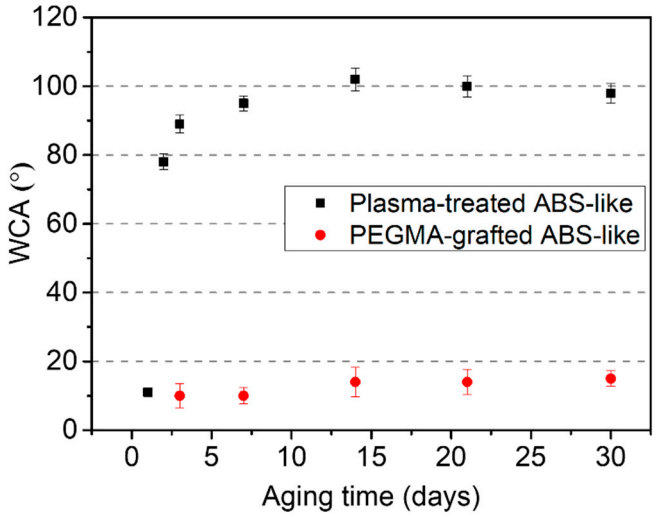

Figure 4. The plot of water contact angle versus aging times.

For further experiments to generate gradient wettability, the flat ABS-like substrate is altered surface by atmospheric pressure plasma at an inclined angle of 20°, the contact angle plotted with their respective working distances is shown in Figure 5, which go along with the CCD images to illustrate the water droplet behavior on these positions. In general, the trend in contact angle increases gradually from 9.5° to 67.7° relating to the working distance in the range of 1.9mm-17.2mm, which means droplets deposited on the gradient surface can propagate in the same direction (Figure 5a). In the following procedure, PEGMA is grafted onto the plasma-treated sample in order to improve the efficiency and durability of hydrophilicity. Figure 5b illustrates the increase in the contact angle from 12.1° to 57.1° with a rising working distance from 3.4mm to 15.4mm. In terms of dynamic wetting behavior, the droplets drop respectively at positions of 23 mm, 30mm, and 44mm in Figure 6. The droplet embarks on spreading at the hydrophilic end and then wets unidirectionally towards the hydrophobic end with traveling distances of 3.59mm, 4.83mm and 6.01mm, respectively.

Preprints.org (www.preprints.org) | NOT PEER-REVIEWED | Posted: 14 May 2024 doi:10.20944/preprints202405.0926.v1

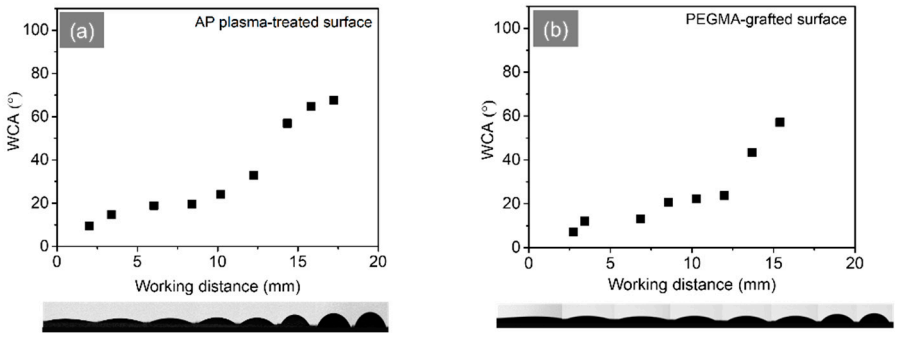

Figure 5. Plot of water contact angles versus the working distance corresponding to the gradient wettability from CCD images. Flat ABS-like samples were prepared and treated by (**a**) AP plasma at an inclined angle of 20°; (**b**) Followed by PEGMS-grafted. The water droplet is 2μL.

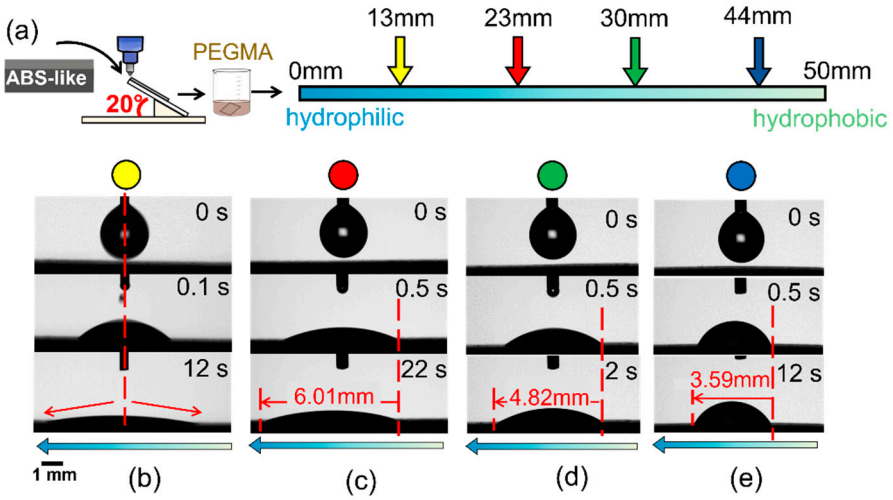

Figure 6. (**a**) The schematic diagram illustrates the surface modification process and the location corresponding to the deposition of droplets on the PEGMA-grafted ABS-like surface. The unidirectional wetting behavior at the position of (**b**) 13mm; (**c**) 23mm; (**d**) 30mm; (**e**) 44mm. the blue arrow indicates the wettable gradient force. The water droplet volume is 5μL.

3.1.2. Chemical Composition Analysis

The ESCA technique is utilized to verify the change in chemical components of modified surfaces. In accordance with the spectra in Figure 7, the peak fitted narrow scan C1s spectrum of the untreated ABS-like surface is compared to that of PEGMA-grafted ones with two specific working distances. Regarding the XPS C1s spectra of untreated surfaces, three peaks are examined including C-C and C-Si bonds at 284.6 eV, C-O or C≡N bonds at the peak of 286.1 eV, and R-O-C=O carboxylic groups or imide groups at the peak of 288.8 eV. Before being grafted by PEGMA solution, plasma treatment at working distances of 3.6 mm and 14.4 mm is conducted separately to observe the alternation in terms of chemical composition. The peak intensity at 286.1 eV conspicuously increases which is caused by the formation of C-O bonds of PEGMA. Additionally, the existence of C-O and C≡N at the intensity of 286.1 eV is associated with reducing working distance, pointing out that the ABS-like surface is placed near the plasma jet improving the bonding formation for the grafting process.

Preprints.org (www.preprints.org) | NOT PEER-REVIEWED | Posted: 14 May 2024 doi:10.20944/preprints202405.0926.v1

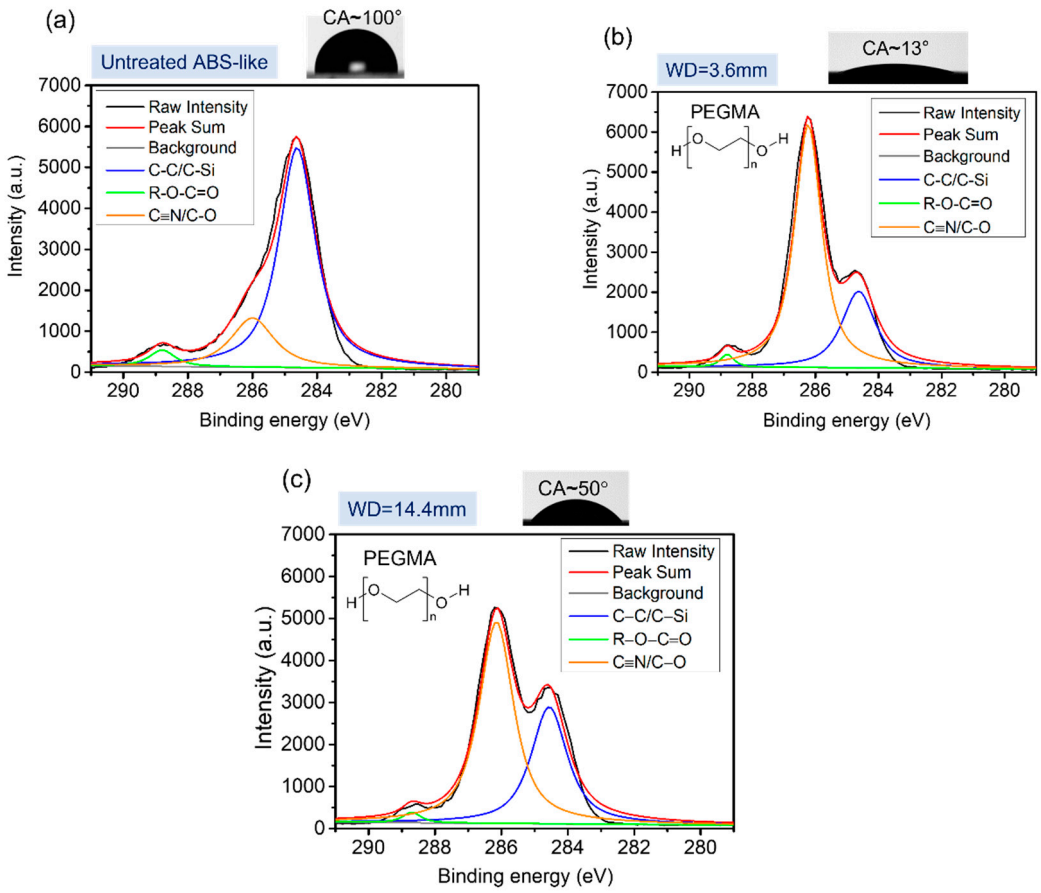

Figure 7. ESCA spectrum of C1s for (a) untreated ABS-like substrate; PEGMA-grafted ABS-like substrate at a working distance of (**b**) 3.6mm; (**c**) 14.4mm.

3.2. Dynamic Wetting Behavior on Multi-gradient 3D-printed Triangular Prism Patterns

The triangular prism groove obsesses a unique way to drive droplets from the high Laplace pressure to the less Laplace pressure regions, which is discovered through barbs of cactus and spider silk in Figure 1 [12,17]. According to the aforementioned results, the sample with triangular prism grooves is treated by AP plasma at an inclined angle of 20° and thenceforth PEGMA grafting to synthesize multi-gradient surfaces. Consequently, two driving forces exist on the pattern to support the droplet for self-transport. The design parameters and laser confocal images of the pattern are shown in Figure 8, the accuracy in thickness and length of the printed ABS-like samples reaches over 98% in comparison to the model in Figure S1.

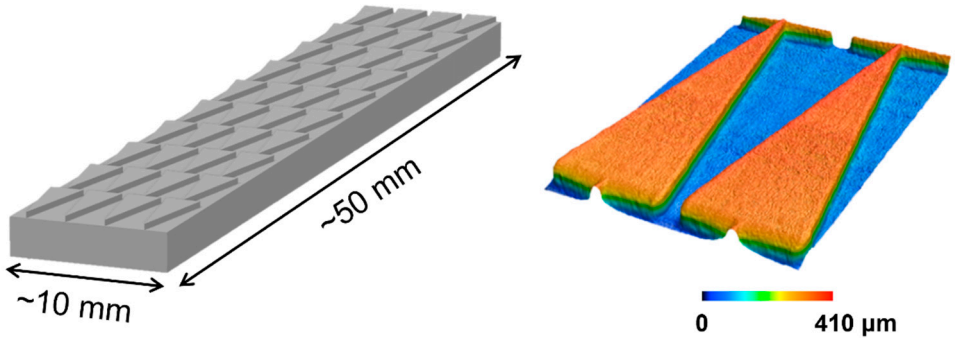

Figure 8. 3D printed ABS-like with triangular prism array and the laser confocal images (color image) showing the structure contour difference design structure (grey image).

 doi:10.20944/preprints202405.0926.v1

The optimal design for manipulating effectively the water self-transport has been investigated by adjusting the thickness (T) and the spacing (S) of the modified samples. Figure 9 shows a series of frames depicting their wetting behavior on different samples. For the samples with a thickness of 0.1 mm and varied spacing (0-0.5mm), the droplets only fill a groove (5mm) at the initial position, because the drop seems to be blocked by the groove's base plane. The samples with a thickness of 0.3-0.5mm contrarily show a decrease in traveling distance with increasing spacing between adjacent patterns (S=0.3-0.5mm), due to the Laplace pressure force being inversely proportional to the triangle radius [30]. As a result, the longest traveling distance of 26.7mm is observed on the pattern with 0.3mm in thickness and 0.3mm in spacing, which is selected as an optimized dimension for the following experiments.

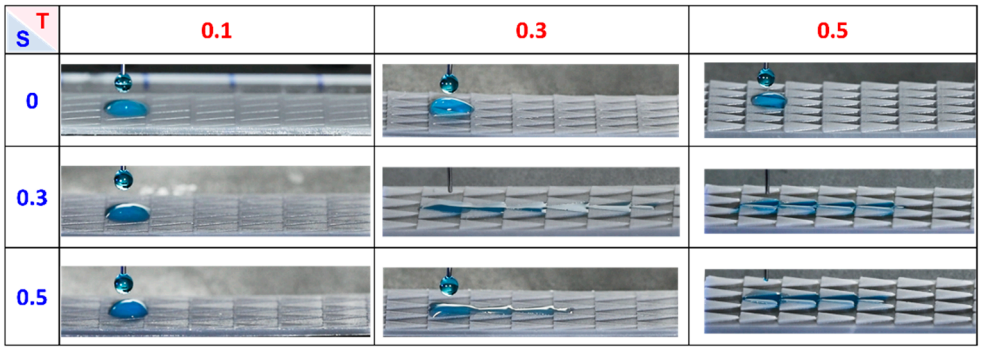

Figure 9. The traveling distance of a droplet on the different samples corresponding to each CCD image. T is defined as the thickness of the triangular prism groove. S is defined as the spacing between each pattern. The volume of a water droplet is 10μL.

Furthermore, the wetting process on the modified pattern with an optimized parameter is entered into detail in Figure 11, the volume droplet of 5μL is deposited on a groove of the hydrophobic side and the water droplet flows 18.47mm along the groove column within 6 seconds. Surprisingly, the result is much higher than that of the untreated (in the hydrophobic state) and uniform hydrophilic 3D-printed triangular prism pattern with 2.6mm and 8.8mm, as shown in Figure 10. The significant change in droplet velocity during the process is analyzed in Figure 11b, owing to the principle of Laplace pressure force, the droplet accelerates near the triangle's tip region and then steadily retards as it reaches the rear region. Similarly, the wetting behavior is observed as the increase in droplet volume to 10μL and 15μL, as shown in Figure 12 and Figure S2. For the case of 10μL, the droplet fills another three grooves longer than that of 5μL in volume, hence the traveling distance extends from 18.47mm to 26.51mm. While a distance of 43.97mm is witnessed with 15μL in water volume, almost approaches the other end of the hydrophilic region.

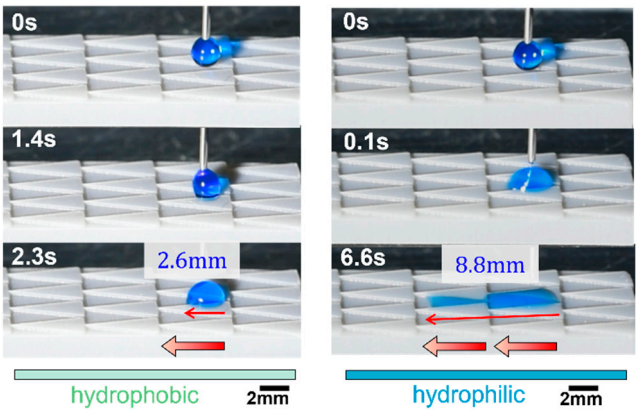

Figure 10. The dynamic wetting behavior on 3D printed triangular prism samples. The lighter blue and darker blue indicate the hydrophobic and hydrophilic surfaces, respectively. The red arrow indicates the direction of water flow. The droplet volume is 5μL.

 doi:10.20944/preprints202405.0926.v1

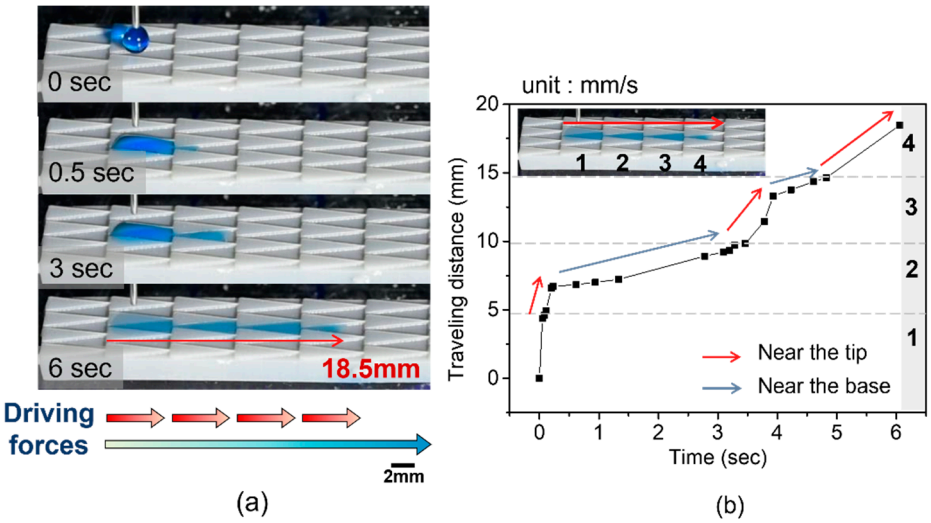

Figure 11. (**a**) The unidirectional spreading behavior on the multi-gradient surface. The blue and red arrows show the trend of water flow driven by the wettable gradient force and Laplace pressure gradient force, respectively. The volume of a water droplet is 5μL; (**b**) The droplet of the traveling distance versus time on the multi-gradient surface. The numbers 1-4 are designated as groove order.

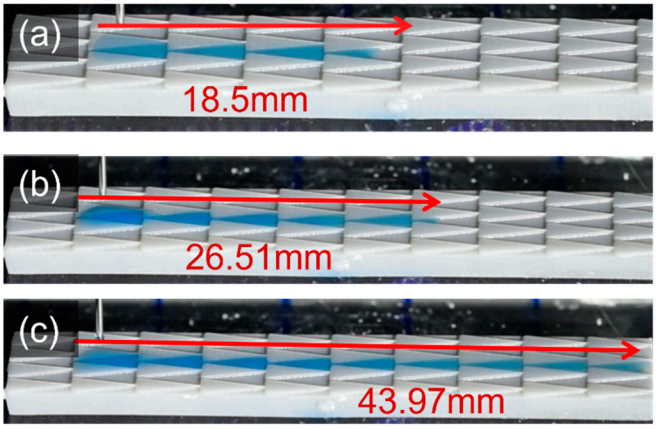

Figure 12. The unidirectional wetting behavior on the multi-gradient surface. The volume of a droplet is (**a**) 5μL; (**b**) 10μL; (**c**) 15μL.

In further investigation, the multi-gradient pattern carries out the anti-gravity trial, and the stage of the contact angle apparatus is set up titling at 10°, 20°, 30°, and 40°. Figure 13 and Figure S3 show a summary of the results that water droplets with 5μL, 10μL, and 15μL wet against gravity at various tilting angles. Regarding the tilting angle of 10° in Figure 13a, the droplet climbs up to 17.57mm with 5μL in volume, the traveling distance is 0.95 times shorter than the case without inclination. The volume of a droplet rises to 10μL and 15μL, which allows it to flow longer with 25.92mm and 40.48mm, respectively. It is seen that the self-transport efficiency can be retained at over 92% in comparison to the non-inclination cases (18.47mm for 5μL, 26.51mm for 10μL and 43.97mm for 15μL). As the titling angle is set to be 20° in Figure 13b, the droplets of 5μL, 10μL, and 15μL correspond to 17.15mm, 22.75mm and 36.34mm in distance against gravity, respectively. Consequently, the efficiency of self-transport is realized at 83% compared to the cases of the horizontal plane, except for the droplet volume of 5μL that can be kept at 93% in efficiency. In terms of 30° in Figure 13c, the anti-gravity process is recorded with an insignificant value of 6.39mm for 5μL and 12.53mm for 10μL in traveling distance. Unfortunately, the multi-gradient force of the triangular prism pattern is no longer against gravity when 15μL in volume is loaded on the pattern, causing the drop partially to run down. To sum up, the anti-gravity water flow is confirmed on the multi-gradient surface, the

 doi:10.20944/preprints202405.0926.v1

integration of the Laplace pressure gradient and the wettable gradient is sufficient to drive the droplet running uphill along the channel from 10° to 30° inclination.

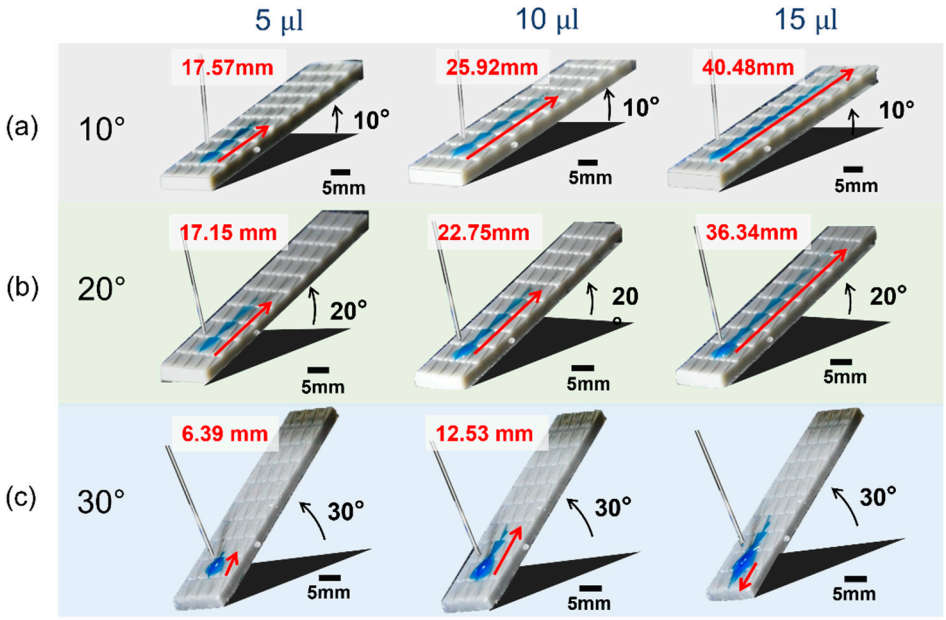

Figure 13. The anti-gravity water flows on the multi-gradient surface. The tilting angle is set to be (a) 10°; (b) 20°; (c) 30° with the droplet volume is 5µL, 10µL, and 15µL.

4. Conclusions

The combination of gradient wettability and Laplace pressure gradient improves the self-transport unidirectionally without any external energy. In this research, we fabricated a substrate with a series of triangular prism grooves by 3D printing, followed by a simple and controllable two-step process to generate a multi-gradient surface. The wettable gradient surface was elucidated by measuring the static contact angle at different positions on the substrate and inspecting the change in chemical composition. Two primary results are mentioned in this study: First, the traveling distance of 18.47mm for 5µL on the multi-gradient surface is 2.1 times, 5.1 times, and 7.1 times higher than the hydrophilic structural surface (8.8mm with Laplace pressure gradient only), flat gradient surface (3.59mm with wettable gradient only), and hydrophobic structural surface (2.6mm with Laplace pressure gradient only). Secondly, water droplets of 5µL to 10µL in volume can run uphill up to a 30° tilting angle, while the droplet with 15µL could against gravity up to an angle of 20°. Such a design offers great potential in transporting small water droplets and anti-gravity, which could be further applied in microfluidic or drainage tubes.

Supplementary Materials: The following supporting information can be downloaded at: Preprints.org, Figure S1: Laser confocal images showing the actual spacing (0, 0.1, 0.3, 0.5, 0.8, 1.2mm from left to right) and the actual thickness (0.1, 0.3, 0.5, 0.8, 1.2mm from top to bottom) of the printed samples; Figure S2: (a) Plot of the traveling distances versus time on the multi-gradient surface. The numbers 1-3 labeled are associated with each triangular prism position, (b) Plot of the traveling distances versus time on the multi-gradient surface. The numbers 1-4 labeled are associated with each triangular prism groove; Figure S3: Plots of the traveling distance versus the tilt angle. The volume of the water droplet is (a) 5µL, (b) 10µL, (c) 15µL; Video S1: title.

References

1. Gau, H.; Herminghaus, S.; Lenz, P.; Lipowsky, R. Liquid morphologies on structured surfaces: from microchannels to microchips. *Science* **1999**, *283*, 46-49.
2. Yao, X.; Song, Y.; Jiang, L. Applications of Bio-Inspired Special Wettable Surfaces. *Adv. Mater* **2011**, *23*, 719-734.

3. Hancock, M.J.; Sekeroglu, K.; Demirel, M.C. Bioinspired directional surfaces for adhesion, wetting, and transport. *Adv. Funct. Mater*. **2012**, *22*, 2223-2234.
4. Ueda, E.; Levkin, P.A. Emerging applications of superhydrophilic- superhydrophobic micropatterns. *Adv. Mater*. **2013**, *25*, 1234-1247.
5. Liu, Y.; Andrew, M.; Li, J.; Yeomans, J.M.; Wang, Z. Symmetry breaking in drop bouncing on curved surfaces. *Nat. Commun.* **2015**, *6*, 10034.
6. Zheng, Y.; Bai, H.; Huang, Z.; Tian, X.; Ni, F.Q.; Zhao, Y.; Jiang, L. Directional water collection on wetted spider silk. *Nature* **2010**, *463*, 640-643.
7. Andrews, H.G.; Eccles, E.A.; Scho, W. C. E.; Badyal. J. P. S. Three-dimensional hierarchical structures for fog harvesting. *Langmuir* **2011**, *27*, 3798-3802.
8. Dong, H.; Wang, N.; Wang, L.; Bai, H.; Wu, J.; Zheng, Y.; Zhao, Y.; Jiang, L. Bioinspired electrospin knotted microfibers for fog harvesting. *ChemPhysChem* **2012**, *13*, 1153-1156.
9. Suzuno, K.; Ueyama, D.; Branicki, M.; Tóth, R.; Braun, A.; Lagzi, I. Maze solving using fatty acid chemistry. *Langmuir* **2014**, *30*, 9251-9255.
10. Schellenberger, F.; Encinas, N.; Vollmer, D.; Butt, H. J. How water advances on superhydrophobic surfaces. Am. *Phys. Soc.* **2016**, *116*, 096101.
11. Park, K. C.; Kim, P.; Grinthal, A.; He, N.; Fox, D.; Weaver, J. C.; Aizenberg, J. Condensation on slippery asymmetric bumps. *Nature* **2016**, *531*, 78-82.
12. Ju, J.; Bai, H.; Zheng, Y.; Zhao, T.; Fang, R.; Jiang, L. A multi-structural and multi-functional integrated fog collection system in cactus. *Nat. Commun.* **2012**, *3*, 1246-1247.
13. Feng, S.; Wang, S.; Gao, L.; Li, G.; Hou, Y.; Zheng, Y. Controlled directional water-droplet spreading on a high-adhesion surface. *Angew. Chem.* **2014**, *126*, 6277-6281.
14. Feng, S.; Wang, S.; Liu, C.; Zheng, Y.; Hou. Y. Controlled droplet transport on a gradient adhesion surface. *Chem. Commun.* **2015**, *51*, 6010-6013.
15. Deng, S.; Shang, W.; Feng, S.; Zhu, S.; Xing, Y.; Li, D.; Hou, Y.; Zheng. Y. Controlled droplet transport to target on a high adhesion surface with multi-gradients. *Sci. Rep.* **2017**, *7*, 45687.
16. Ogburn, R. M.; Edwards, E. J. Anatomical variation in Cactaceae and relatives: Trait lability and evolutionary innovation. *Am. J. Bot.* **2009**, *96*, 391-408.
17. Shanyengana, E.S.; Henschel, J. R.; Seely, M. K.; Sanderson R. D. Exploring fog as a supplementary water source in Namibia. *Atmos. Res.* **2002**, *64*, 251-259.
18. Chen, W.; Guo, Z. Hierarchical fibers for water collection inspired by spider silk. *Nanoscale* **2019**, *11*, 15448-15463.
19. Brown, P.S.; Bhushan, M. Bioinspired materials for water supply and management: water collection, water purification and separation of water from oil. *Phil. Trans. R. Soc. A.* **2016**, *374*, 20160135.
20. Wu, J.; Yan, Z.; Yan, Y.; Li, C.; Dai, J. Beetle-inspired dual-directional Janus pumps with interfacial asymmetric wettability for enhancing fog harvesting. *ACS Appl. Mater. Interfaces.* **2022**, *14*, 49338-49351.
21. Bai, H.; Tian, X.; Zheng, Y.; Ju, Y.; Zhao, J.; Jiang, L. Directional controlled driving of tiny water drops on bioinspired artificial spider silks. *Adv. Mater*. **2010**, *22*, 5521-5525.
22. Malvadkar, N. A.; Hancock, M. J.; Sekeroglu, K.; Dressick, W. J.; Demirel, M. C. An engineered anisotropic nanofilm with unidirectional wetting properties. *Nat. Mater.* **2010**, *9*, 1023-1028.
23. Xue, Y.; Chen, Y.; Wang, T.; Jiang, L.; Zheng, Y. Directional size-triggered microdroplet target transport on gradient-step fibers. *J. Mater. Chem. A.* **2014**, *2*, 7156-7160.
24. Wang, Q.; Meng, Q.; Chen, M.; Liu, H.; Jiang, L. Bio-inspired multistructured conical copper wires for highly efficient liquid manipulation. *ACS Nano* **2014**, *8*, 8757-8764.
25. Zhang, M.; Wang, L.; Hou, Y.; Shi, W.; Feng, S.; Zheng, Y. Controlled smart anisotropic unidirectional spreading of droplet on a fibrous surface. *ACS Nano* **2015**, *9*, 4362-4370.
26. Zhang, M.; Wang, L.; Hou, Y.; Shi, W.; Feng, S.; Zheng, Y. Controlled smart anisotropic unidirectional spreading of droplet on a fibrous surface. *Adv. Mater*. **2015**, *27*, 5027-5062.
27. Zhu, H.; Yang, F.; Li, J.; Guo, Z. High-efficiency water collection on biomimetic material with superwettable patterns. *Chem. Commun.* **2016**, *52*, 12415-12417.
28. Deng, S.; Shang, W.; Feng, S.; Zhu, S.; Xing, Y.; Li, D.; Zheng, Y. Controlled droplet transport to target on a high adhesion surface with multi-gradients. *Sci. Rep*. **2017**, *7*, 45687.
29. Kim, H. T.; Jeong, O. C. PDMS surface modification using atmospheric pressure plasma. *Microelectron. Eng*. **2011**, *88*, 2281-2285

 doi:10.20944/preprints202405.0926.v1

30. Lorenceau, E.; Quéré, D. Drops on a conical wire. *J. Fluid Mech*. **2004**, *510*, 29-45.